Hindawi
Journal of Chemistry
Volume 2022, Article ID 6884947, 11 pages
https://doi.org/10.1155/2022/6884947

Research Article

Synthesis of Spherical Composite CMC-LTO-EGDE-ME for Lithium Recovery from Geothermal Water

Yingchun Xie,[1,3] Yilin Zhang,[2] Jiayu Qin,[2] Murodjon Samadiy,[2,4] and Tianlong Deng[2]

[1]*School of Environmental Science and Engineering, Tianjin University, Tianjin 300350, China*
[2]*College of Chemical Engineering and Materials Science, Tianjin University of Science and Technology, Tianjin 300457, China*
[3]*CNNP Kunhua Energy Development Co Ltd, Hangzhou 311113, China*
[4]*Department of Chemical Technology and Inorganic Substances, Yangiyer Branch of Tashkent Chemical Technology Institute, Yangiyer 121000, Uzbekistan*

Correspondence should be addressed to Murodjon Samadiy; samadiy@inbox.ru and Tianlong Deng; tldeng@tust.edu.cn

Received 21 March 2022; Revised 30 August 2022; Accepted 25 October 2022; Published 28 November 2022

Academic Editor: Gang Feng

In this study, ethylene glycol diglycidyl ether (EGDE) and melamine (ME) were used to prepare a spherical composite material CMC-LTO-EGDE-ME through the strategy of cross-linking reaction of biodegradable sodium carboxymethyl cellulose (CMC) with Li_2TiO_3 (LTO) to improve the cycle stability of the adsorption-desorption for lithium recovery. In the geothermal water at 333.15°K, the adsorption capacity of the spherical composite adsorbent for lithium-ion is 12.02 mg/g, and the adsorption equilibrium time is 8 h. There is a good selectivity of Li^+ ($K_d = 3.7 \times 10^3$) and high separation factors between Li^+ and Na^+, K^+, Cs^+ and Ca^{2+} (between 39.17 and 181.97). Studies on adsorption kinetics and adsorption isotherm showed that composite material's adsorption process was obtained from the pseudosecond-order kinetics and the molecular diffusion model. It was found that the composite material has broad applications in lithium recovery from geothermal water.

1. Introduction

Lithium is extensively used in lithium-ion batteries (LIBs), pharmaceuticals, aerospace, nuclear, and rocket propellants [1–3]. At the time, LIBs is broadly used in many fields, such as electric vehicles, electronic devices, etc. [4]. The massive consumption of fossil fuels will aggravate environmental pollution with the increasing depletion of solid lithium resources and the high energy consumption in the actual production process [5–7]. Therefore, in recent years, researchers have gradually turned their attention to green and environment-friendly liquid lithium resources, including geothermal fluid, seawater, underground water, and salt lake brine. Although the lithium content is lower than the average in solid lithium ore, its resources are extremely rich, with large reserves, most of which are of great mining value.

In recent decades, a variety of techniques have been reported on lithium recovery from liquid lithium resources, including precipitation [8], crystallization separation [9], solvent extraction [10], electrochemical method [11, 12], adsorption [13], and membrane technology [14]. However, each of these approaches has its drawbacks. For example, evaporative crystallization is one of the most extensively used methods of extracting Li^+ from brine. Still, the evaporation process requires large areas to dry for a long time. Meanwhile, it promotes soil salinization, which will lead to serious environmental problems. Among these extraction methods, the adsorption method has the characteristics of high efficiency, low cost, and good cost-effectiveness. Previously a variety of Li^+ adsorbent materials, including $Al_2O_3\ nH_2O$, $Li_{1\text{-}a}H_aSbO_3$, and $LiCl\ 2Al(OH)_3\ H_2O$, were reported for lithium recovery where the Li^+ selectivity was low or too expensive to apply for economy lithium recovery [15]. Lithium-ion sieves mainly focus on the manganese series and titanium series, and manganese series ion sieves cause a more considerable dissolution loss due to the manganese disproportionation reaction [16]. Among titanium series ion sieves, Li_2TiO_3 (LTO) is easy to synthesize, has a stable structure, high adsorption

capacity, easy elution, and slight dissolution loss, exhibiting excellent lithium adsorption performance [17].

As an environmentally friendly technology for lithium extraction, adsorption has attracted extensive attention from many scientists. The key is synthesizing a kind of adsorption material with high selectivity, stable structure, and moderate particle size that can be used in industry [18]. Adsorption is a method to separate and extract lithium from liquid lithium ore, which is easy to realize in large-scale industrial operations. This technology's core prepares a functional adsorption material with high selectivity, stable structure, and solid industrial application for lithium in solution. Currently, the research on lithium adsorbents mainly focuses on aluminum-based adsorbents and lithium-ion sieve adsorbents (LIS), as well as composite lithium adsorbents synthesized based on powder materials [19]. However, the main limitations for commercial applications of LIS are structural strength and loss of dissolution during column adsorption. Therefore, researchers have tried to make composites by combining powdered materials with spheres, foams, and membranes [20, 21]. However, stabilization of LIS is more challenging; the capacity and speed of powdered LIS will substantially decrease [22, 23]. In short, for a commercial LIS process, the key is to minimize the dissolution losses of powdered materials and thereby prevent a decrease in adsorption characteristics. Currently, immobilization of LTO particles in polymers is an important goal that may allow these particles to be applied to large-scale applications. Due to the organic polymer carboxymethylcellulose (CMC) biopolymer having solubility, biocompatibility, and nontoxicity, it is considered a reasonable candidate for immobilization [24]. In addition, when the ions of Fe^{3+}, Cu^{2+}, La^{3+}, and Al^{3+} exist [25], the CMC's chemical structure is shown in Figure 1.

With an iron chloride cross-linked sodium carboxymethylcellulose (CMC) biopolymer and melamine (ME) as an immobilized matrix, a novel environmental-friendly adsorbent CMC-LTO-EGDE-ME was prepared to recover lithium from geothermal water. CMC-LTO-EGDE-ME composite spheres were designed at room temperature using only environmentally friendly materials. XRD, SEM, and FT-IR characterized the extraction mechanism of absorbent. Besides, the adsorption isotherm and kinetic model of lithium in geothermal water are studied, and the adsorption capacity of lithium in geothermal water under different experimental conditions is evaluated in detail.

2. Materials and Methods

2.1. Reagents and Materials. Lithium chloride (LiCl 98%), lithium carbonate ($LiCO_3$ 98%), titanium dioxide (TiO_2, 99%), hydrochloric acid (HCl 36%), and caustic soda (NaOH 96%) were sourced from the Shanghai Aladdin Biochemical Technology Co., Ltd. Monohydrate lithium hydroxide (LiOH H_2O, 98%) was obtained from the Shanghai Hushi environmental protection reagent Technology Co., Ltd. Sodium carboxymethyl cellulose (CMC, $n = 1050$) was obtained from Tokyo Chemical Industry Co., LTD. Ethylene glycol diglycidyl ether (EGDE, 99%) and melamine (ME, 99%) were produced by Shanghai Linens Technology Development Co., LTD.

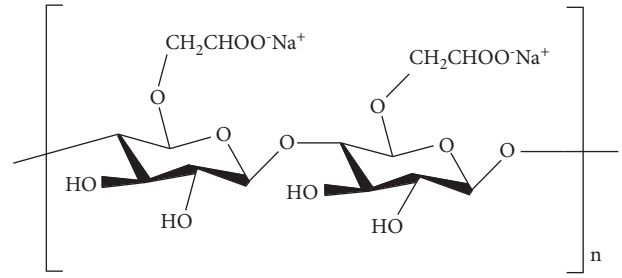

Figure 1: Structure formula of CMC.

In addition, the conductive double-deionized water (DDW, $<1 \times 10^{-4}$ S/M at 298.15°K) was used to prepare the solutions. The geothermal water was sampled from Tibet, and its composition is shown in Table 1.

2.2. Experiment Methods

2.2.1. Synthesis of Absorbent Li_2TiO_3. The hydrothermal and modified solid-phase calcination methods were used to synthesize the Li_2TiO_3 precursor. As to the modified solid-phase calcination methods, 1 mol of Li_2CO_3 and 1 mol of anatase-type TiO_2 were mixed with absolute ethyl alcohol for about 2 h after drying and grinding. Then, LTO-1 was obtained by reaction at 1023°K for 7.5 h in a muffle furnace (SG-GS1200, Shanghai, China) and grinding after cooling to room temperature. As to the hydrothermal method, 0.167 mol of anatase-type TiO_2 and 0.2 mol of LiOH H_2O were mixed with absolute ethanol and then placed in an autoclave lined with Teflon, then stirred and heated for 24 h at 433°K. After the reaction was finished, it was cooled down to room temperature, filtered, and reacted in a muffle furnace at 773°K for 3 h. Then, the product was grounded after cooling and named LTO-2.

2.2.2. The Spheres of CMC-LTO and CMC-LTO-EDGE-ME Preparation. 1.5 g Li_2TiO_3, 1.5 g CMC, and 100 mL of DDW were added into the breaker, stirred at room temperature for about 6 h, and a homogeneous solution was obtained by sonication for several minutes. Next, the mixed solution was dripped and stirred continuously until 100 mL of a 2 wt% $FeCl_3$ solution, and then the solidified CMC-LTO was constantly stirred for about 12 h. The CMC-LTO pellets were then washed several times with DDW until Fe (III) ions were free.

The prepared CMC-LTO microspheres were placed in 2 wt% ethylene glycol diglycidyl ether (EDGE) and reacted at 318.15°K for 6 h, which could make the hydroxyl group fully modified. After 6 h, the EDGE on the surface of the spheres was removed with deionized water.

After filtration, the CMC-LTO-EGDE spheres were placed in a 2% melamine (ME) solution and mechanically stirred at a constant rate at 318.15°K for 6 h to allow complete cross-linking. After standing for 6 h, the spheres were filtered, and a sufficient amount of deionized water was used to

Table 1: Chemical composition of the geothermal water sample.

pH	Composition ($mg{\cdot}L^{-1}$)							
	Li^+	Na^+	K^+	Rb^+	Cs^+	Ca^{2+}	Cl^-	B_2O_3
8.80	25.78	682.01	137.9	3.45	17.58	211.05	973.06	360.16

remove residual ME on the surface of the spheres. Then, the CMC-LTO-EGDE-ME material was finally obtained after vacuum drying at 318.15°K for 24 h. The preparation process of the spherical composite shows in Figure 2.

2.2.3. Lithium Adsorption from Geothermal Water by CMC-LTO-EGDE-ME. Adjusted the pH of the solution at 12.0, and CMC-LTO-EGDE-ME adsorbed Li^+ at 318.15°K. The contents of Li^+, Na^+, K^+, Cs^+, and Ca^{2+} in the solution before and after adsorption were determined by ICP-OES (Prodigy, Leeman, USA). The adsorption-desorption cycle evaluated the stability of porous CMC-HTO-EGDE-ME (HTO, H_2TiO_3). 0.25 mol/L HCl was used as an adsorption solution, and then the adsorbent was also regenerated by elution for 2 h.

The adsorption performances of the adsorbent can be evaluated by distributing the coefficient (K_d), separating coefficient ($\alpha Li/Me$), adsorption capacity (q), adsorption rate (E), and elution rate (DE). Therefore, the definitions are in the following equation:

$$
\begin{aligned}
K_d &= \frac{C0 - Ce}{Ce} \times \frac{V1}{m1}, \\
\alpha_{Me}^{Li} &= \frac{K\,d\,(Li)}{K\,d\,(Me)}, \\
q_{Li} &= \frac{(C0 - Ce)V1}{m1}, \\
E_{Li}\,(\%) &= \frac{C0 - Ce}{C0} \times 100, \\
DE_{Li}\,(\%) &= \frac{C1 - V2}{m2} \times 100,
\end{aligned}
\tag{1}
$$

where $c_{0,}c_{e,}$ and c_1 (in mg/L) express the Li^+ contents in initial, equilibrium, and eluent solutions, respectively; m_1 and m_2 (g) present the amount of adsorbent used and the adsorbed lithium by the adsorbent; V_1 (L) is the geothermal water volume, and V_2 (L) is the volume of the eluate.

3. Results and Discussion

3.1. Adsorption Properties of the Synthesized HTO by Different Methods. Figure 3 compares the XRD patterns and particle size distributions for the two precursors of LTO-1 and LTO-2. And then, the precursors LTO-1 and LTO-2 were removed as HTO with 0.25 mol/L HCl. Next, HTO was eluted using 0.25 mol/L HCl for approximately 12 h.

0.1 g of HTO was adsorbed in 100 mL of 20 mg/L Li^+ solutions for 6 h at 318.15°K and pH = 12. Figure 3(a) shows that the LTO-1 and LTO-2 XRD patterns agree well with the standard patterns of LTO. However, the solid-phase calcination method can be synthesized in large quantities, and the synthesis conditions are relatively simple. While for the hydrothermal synthesis method, the product has a small particle size and less agglomeration. In Figure 3(b), the average particle sizes of LTO-1 and LTO-2 were 3.769 and 92.642 μm. However, under the same conditions, the adsorption capacity (q_{Li}) of HTO-1 was 2.6 times higher than that of HTO-2. Therefore, LTO precursors prepared by solid-phase calcination perform better than those prepared by the hydrothermal method.

3.2. Particle CMC-LTO-EGDE-ME Adsorbs Li^+

3.2.1. Granulation Effect on Adsorption Properties. The mechanism of lithium-ion exchange by HTO can be expressed as follows:

$$H_2TiO_3 + 2Li^+ = Li_2TiO_3 + 2H^+. \tag{2}$$

The effects of pH, dosage, and temperature on adsorption and elution before granulation were investigated. The results show in Figure 4. It can be seen in Figure 4(a) that pH value had a significant effect on HTO-1 adsorption. For example, when pH equals 12.0, HTO-1 has the best adsorption capacity for lithium ions. When the pH value is higher than 12.0, Li^+ exchange is blocked, and agglomeration occurs on the surface. As a result, the adsorption rate increases with the amount of adsorbent, while the adsorption capacity (q_{Li}) is the opposite in Figure 4(b). And when the dosage is higher than 1.3 g/L, the HTO-1 adsorption efficiency reaches almost 100%. Therefore, the solid-liquid ratio of 2.0 and pH 12.0 was selected for Li^+ absorption and an initial Li^+ concentration of 20 mg/L. In Figure 4(c), the Li^+ desorption rate of LTO-1 increases with the increase in temperature. In Figure 4(d), the Ti^{4+} dissolution loss in the solution increases dramatically with the increase of HCl concentrations. Therefore, to maintain the adsorbent's stability, the optimal eluent acidity was chosen as 0.25 mol/L HCl.

3.2.2. Cross-Link Methods. CMC is a hydrophilic macromolecular because there are free hydroxyl and carboxyl in the structure of CMC, which affects its stability of CMC. So, modify the molecular structure of CMC through the cross-linking strategy for the hydroxyl groups to increase the hydroxy implementation "concealed effect" and its stability. Ethylene glycol glycidyl ether (EGDE) has an epoxy group at both ends of the molecule and can react with amino, hydroxyl, carboxyl, and other active groups. The CMC-LTO microspheres formed by cross-linking CMC and LTO solution using Fe^{3+} contain a large number of free hydroxyl groups. In a neutral or weak acidic environment (pH 6.5–7), the ring-opening reaction can occur with the epoxy groups at both ends of the EGDE molecule to form a three-dimensional network structure. The reaction principle is shown in Figure 5(a). However, the ring-opening reaction of the EGDE molecule has limited binding efficiency with the free hydroxyl group. Only one end of the epoxy group of some EGDE molecules participates in the response with the hydroxyl group. In contrast, the other end is not bound to the CMC molecule, thus affecting its cross-linking efficiency. Three melamine molecules polymerize melamine (ME). There are

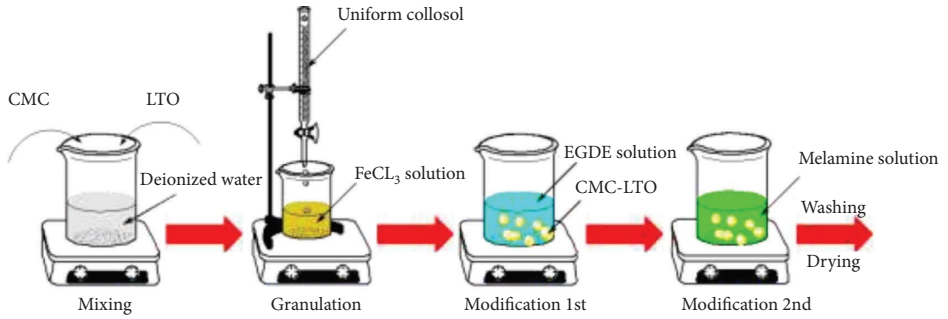

Figure 2: Schematic presentation of CMC-LTO-EGDE-ME microsphere preparation procedure.

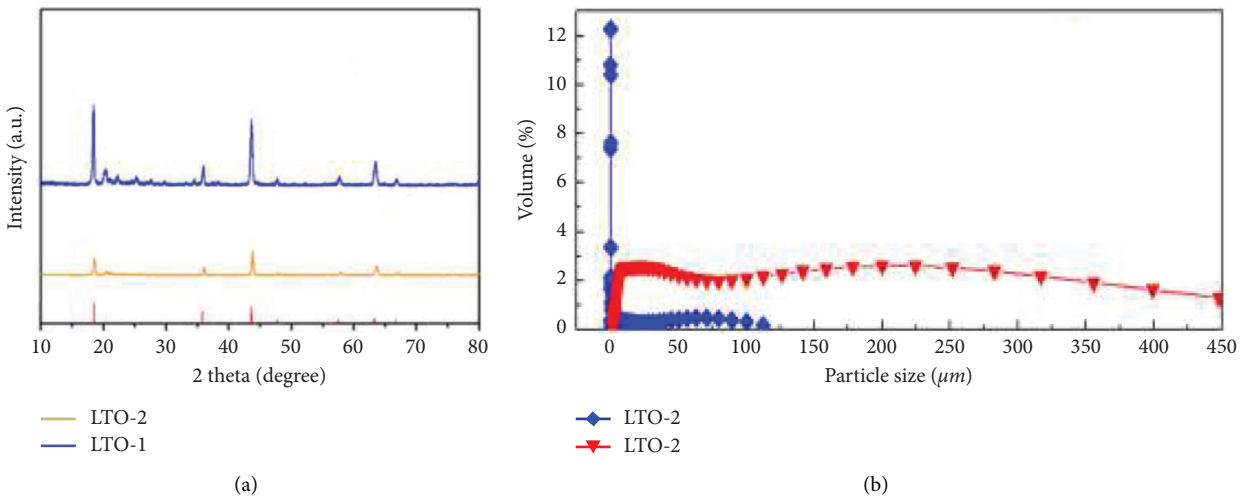

Figure 3: Comparison between LTO-1 and LTO-2. (a) XRD patterns; (b) particle size distribution diagram.

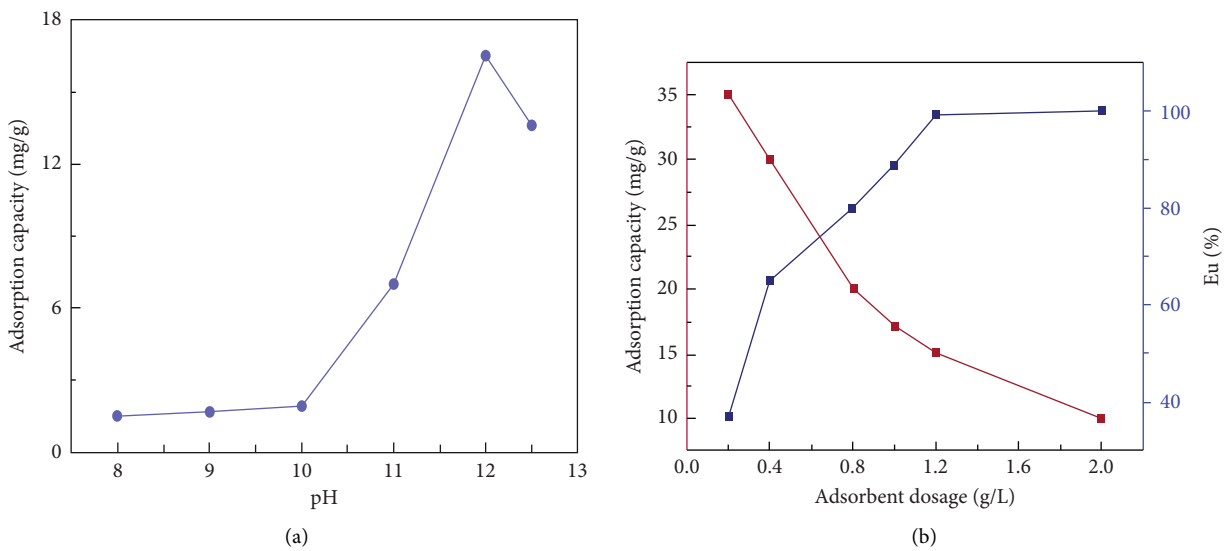

Figure 4: Continued.

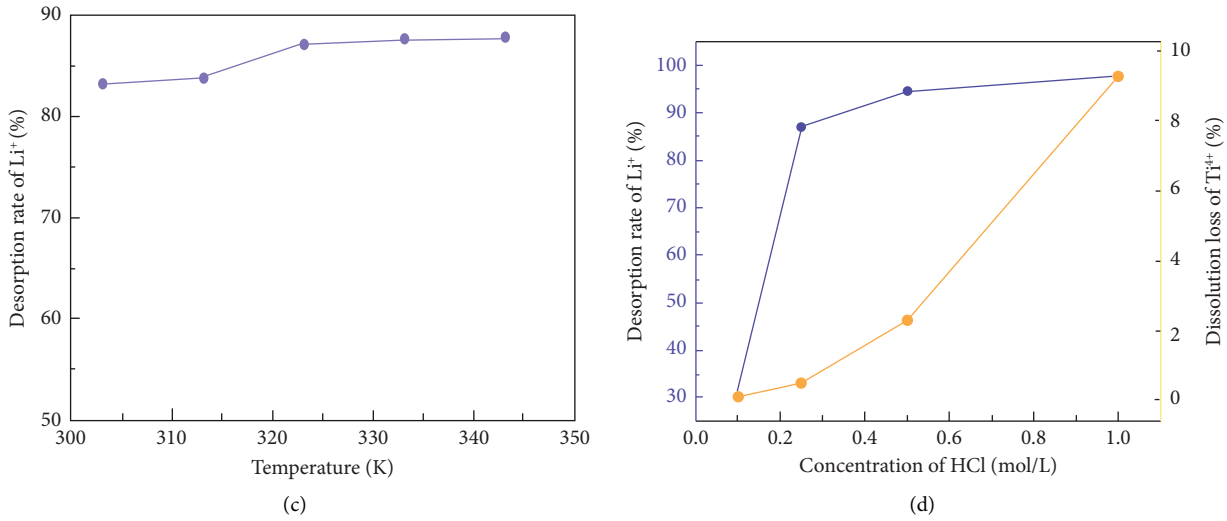

Figure 4: pH (a) and dosage of adsorbent (b) for Li^+ adsorption as well as temperature (c) and chloride acid concentration (d) for Li^+ desorption of HTO-1.

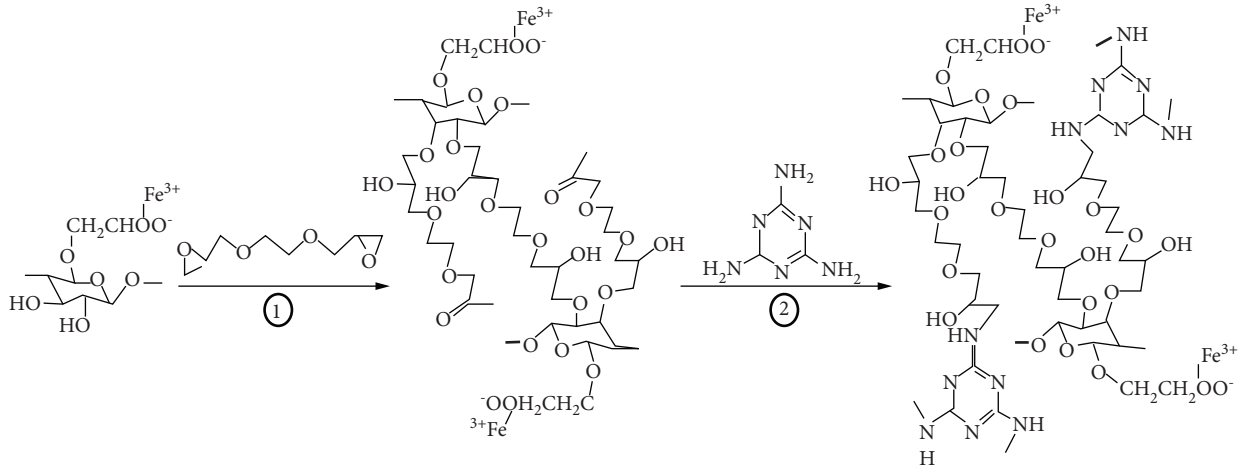

Figure 5: Schematic presentation of CMC cross-linked by EGDE (a) and ME (b).

three active amino groups in the structure of melamine. It can react with hydroxymethyl derivatives to form resin products in a neutral or weakly alkaline environment (pH 7–7.5). So the use of melamine to secondary cross-linking modification, cross-linking reaction as shown in Figure 5(b), the amino group on the melamine molecule reacts with the Schiff base at the other end of the incomplete EGDE epoxy group on the cross-linking reaction, thus forming a stable and tight 3D network structure, thus increasing the stability of the cross-linking mechanism as shown in Figure 5.

3.3. Application of Particles CMC-LTO-EGDE for Li^+ Recovery

3.3.1. Competing Ion Effects on Lithium Adsorption. The selectivity of CMC-LTO-EGDE-ME for Li^+ was investigated for the competing cations (Na^+, K^+, Cs^+, and Ca^{2+}) that coexisted in the solutions. The effect of the coexisted competing cations in geothermal water was studied under pH (12 ± 0.02) at 318.15°K.

Table 1 shows that although the contents of competitive ions in the geothermal water sample are high, the CMC-HTO-EGDE sphere still has a high lithium partition coefficient ($K_d = 3.7 \times 10^3$) in Table 2, higher than the partition coefficient. Furthermore, α (Li/Me) between Li^+ and Me (Me = Na^+, K^+, $Cs^{+,}$ and Ca^{2+}) are higher than 39.17, indicating that CMC-LTO-EGDE-ME microspheres have good selectivity for Li^+.

Table 3 shows the adsorption experiments at different temperatures. The ΔG (kJ/mol), ΔH (kJ/mol), and ΔS (J/mol·K) were obtained according to the experimental results using those calculation formulae.

$$\ln K_d = \frac{\Delta S}{R} - \frac{\Delta H}{RT}, \tag{3}$$

$$\Delta G = \Delta H - T\Delta S. \tag{4}$$

In (3) and (4), K_d represents Li^+ distributive coefficient. T and R are in Kelvin and 8.314 J/mol·K, respectively. The

Table 2: Selectivity of the spheres CMC-LTO-EGDE-ME in geothermal water.

	Li^+	Na^+	K^+	Ca^{2+}	Cs^+
K_d (mL/g)	3766.70	20.70	34.39	96.17	74.83
α (Li/Me)	1.00	181.97	109.53	39.17	50.34

Table 3: Thermodynamic properties of CMC-LTO-EGDE spheres adsorption.

T/K	ΔG (kJ/mol)	ΔH (kJ/mol)	ΔS (J/mol·K)
298.15	−15.15	83.61	331.25
308.15	−18.46		
318.15	−21.86		
328.15	−25.09		

adsorption capacity is raised gradually with temperature increases. In Table 3, the ΔH is greater than 0, indicating the adsorption process is endothermic [26].

3.3.2. FT-IR Characterization Analysis. Figures 6(a) and 6(b) show FT-IR spectra before and after EGDE cross-linking CMC-LTO. At 1733 cm^{-1}, there is an asymmetric stretching peak of -C=O, and at 1733 cm^{-1} shows a characteristic peak of the aldehyde group, indicating that the modification is successful in the first step. Samples of CMC-LTO-EGDE and CMC-LTO-EGDE-ME are shown in Figure 6(c). The broad absorption peaks at 3429 and 3217 cm^{-1} are stretching N-H and O-H vibration peaks. In addition, the stretching vibration peaks of C-N and -RC=N- at 1635 and 1380 cm^{-1} and the disappearance of the aldehyde group characteristic peak of the first cross-linking reaction product CMC-LTO-EGDE at 1733 cm^{-1} also indicated that ME cross-linking was successful.

3.3.3. SEM Analysis. Figures 7(a)–7(d) show the SEM characterization of CMC-LTO-EGDE-ME material. Figure 7(a) shows that CMC-LTO-EGDE-ME is a spherical material in 1–2 mm diameter. In Figures 7(b) and 7(c), the surface of CMC-LTO-EGDE-ME microspheres before adsorption is rough and has a specific pore structure, forming abundant folds on the material surface that is conducive to the adsorption process. As shown in Figure 7(d), a large amount of Li_2TiO_3 powder can be wrapped inside the CMC-LTO-EGDE-ME microsphere, indicating many adsorption sites are conducive to the progress of the adsorption process.

3.3.4. Effect of pH. Figure 8 shows the adsorption influence of geothermal water with different pHs of CMC-HTO-EGDE-ME material. It can be seen that H^+ and Li^+ ions have similar radii and compete with each other for sites on the ion sieve. When pH is lower than 9, the adsorption of Li^+ by the CMC-HTO-EGDE-ME sphere was inhibited, and the adsorption capacity of Li^+ is low. However, when the pH value is higher than 9 and reaches the maximum with pH = 12, the adsorption capacity of the CMC-HTO-EGDE-ME sphere is increased sharply. When the pH value is higher than 12.0,

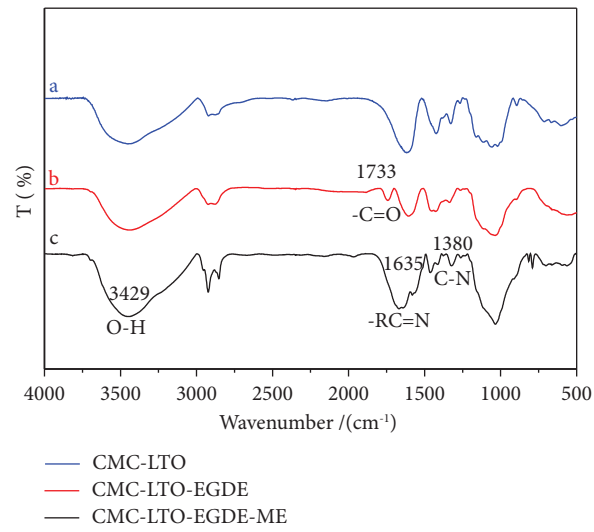

Figure 6: Comparison of FT-IR spectra: (a) CMC-LTO, (b) EGDE cross-linked CMC-LTO, and (c) ME cross-linked CMC-LTO-EGDE.

the ion exchange capacity between H^+ and Li^+ is decreased, and surface agglomeration occurs under highly alkaline conditions.

3.3.5. Adsorption Time. Figure 9 presents the adsorption capacity of lithium is positively correlated with adsorption time by CMC-HTO-EGDE-ME material in geothermal water.

During the adsorption process, the adsorption capacity increased significantly before 8 h, after which the adsorption rate gradually decreased until the adsorption saturation. After 24 h adsorption, the maximum adsorption capacity was 12.02 $mg{\cdot}g^{-1}$. Therefore, the adsorption time of 8 h was selected in the study.

3.3.6. Kinetic Properties of Sphere CMC-LTO-EGDE-ME for Li^+ Adsorption. The kinetic models on pseudofirst-order, pseudosecond-order, and particle diffusion were used as follows [27, 28]:

$$\ln\left(qe - q_t\right) = \ln q_e - k1t,$$
$$\frac{t}{q_t} = \frac{1}{k2q_e2} + \frac{t}{q_e}, \quad (5)$$

where k_1 (h^{-1}) and k_2 (g/mg·h) instead of the rate constants of the first two models. q_e (mg/g) is the equilibrium adsorption capacity, and q_t (mg/g) is the amount of adsorption at any time t. Figure 10(a) plots ln (q_e–q_t) and t. According to its slope and intercept, k_1 and q_e can be calculated. Figure 10(b) shows the plot of t/q_t and t, and the k_2 and q_e can be calculated according to the intercept and the slope. The kinetic parameters of the adsorption process are shown in Table 4.

The intraparticle diffusion model also revealed the adsorption processes [29].

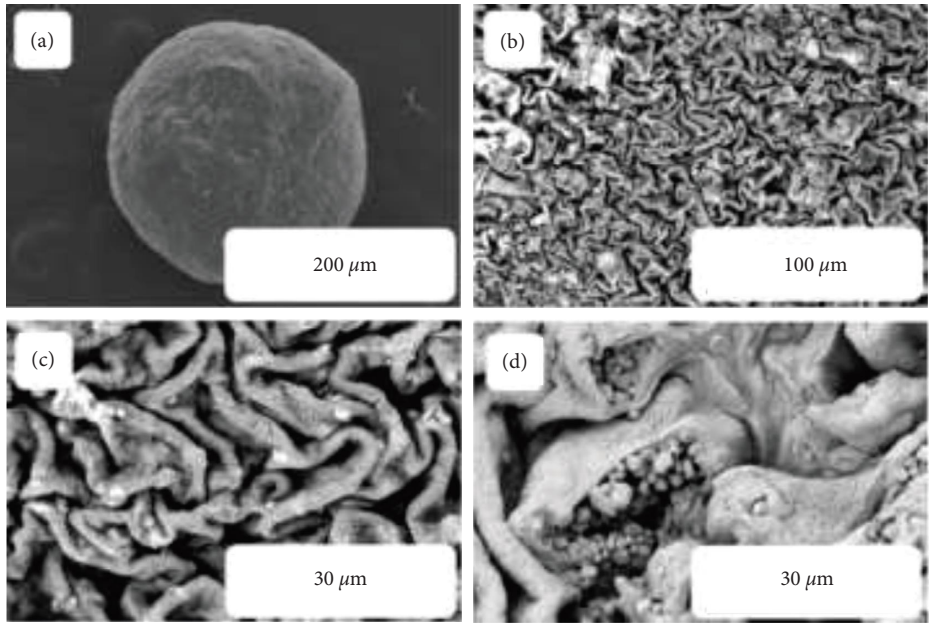

Figure 7: SEM analysis of the samples: (a, b, c, and d) were SEM spectra of CMC-LTO-EGDE-ME.

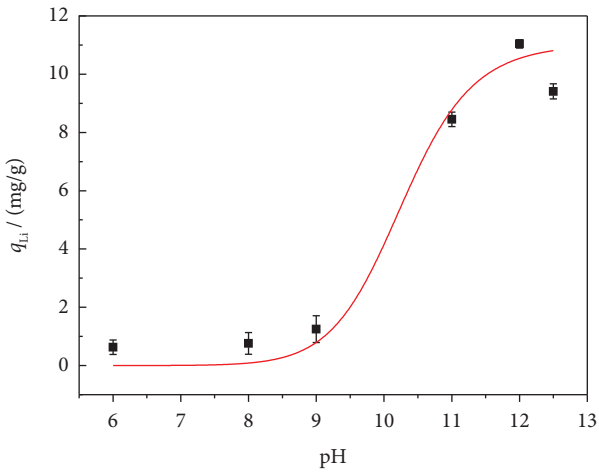

Figure 8: CMC-HTO-EGDE-ME: pH effect for adsorption from geothermal water.

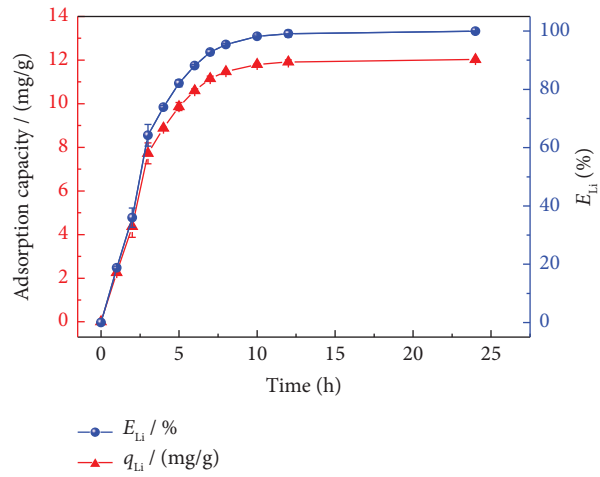

Figure 9: CMC-HTO-EGDE-ME: time effect for Li^+ adsorption from geothermal water.

$$q_t = K_{di\,f} t^{1/2} + C, \tag{6}$$

where K_{dif} (mg/g·h$^{1/2}$) presents the rate constant of the intraparticle diffusion model, and C expresses intercept. Figure 11 shows the results of q_t against $t^{1/2}$.

The correlation coefficient (r) between t/q and t in Figure 11(b) is 0.996. Table 4 shows that the theoretically calculated value (12.90 mg/g) is consistent with the experimental (12.02 mg/g). Therefore, the Li^+ adsorption process of CMC-LTO-EGDE-ME can be described more accurately by the quasi-second-order model.

In Figure 11, the adsorption process can be separated into three stages. In Table 5, the K_{dif} of each stage was fitted, and the relative coefficients (R^2) in the three phases are all higher than 0.98. Stage I represents diffusion from the solution to the microspheres, stage II represents diffusion from the surface to the pores, and stage III represents diffusion within the microspheres.

The diffusion rate constants of the three phases decrease successively, indicating that it is increasingly difficult for Li^+ to bind to the adsorption sites on the microspheres in solution. The diffusion rate constant of phase I is much higher than that of phases II and III, which means that the diffusion rate on the microsphere's surface is much higher than that inside the microsphere, and phase III is the decisive speed step.

3.3.7. Reusability of Sphere CMC-LTO-EGDE-ME. Figure 12 shows the chloride acid as an eluent effect for the desorption rate of lithium-ion and the dissolution rate of Ti^{4+} with different concentrations of hydrochloric acid. The adsorption stability-desorption test evaluated the cycle

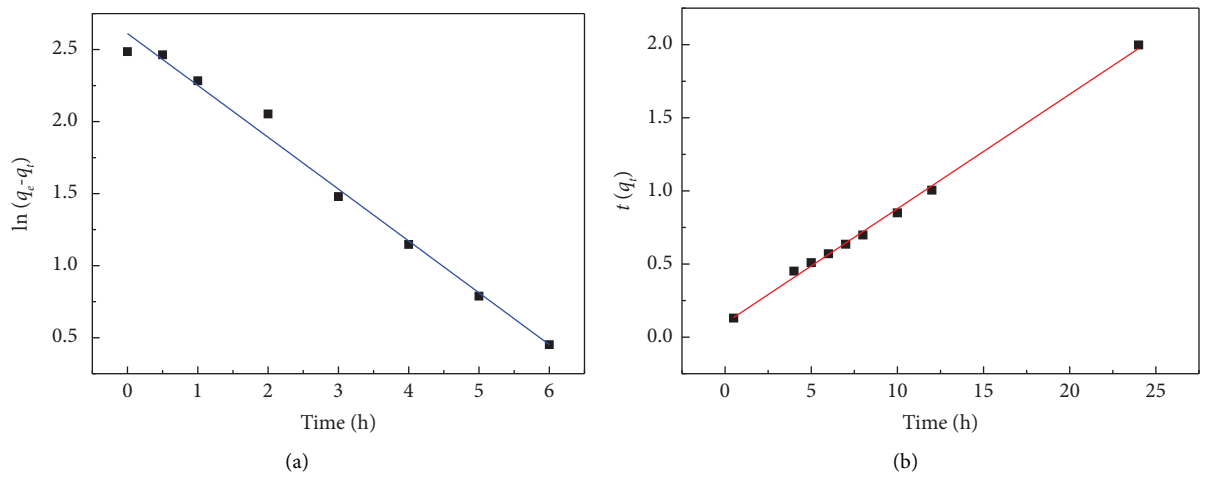

Figure 10: Plotting on pseudofirst-order (a) and pseudosecond-order (b).

Table 4: Relative parameters of the pseudofirst/second-order models.

Experiment	Pseudofirst-order			Pseudosecond-order		
q_e (mg·g^{-1})	q_e (mg·g^{-1})	K_1 (h^{-1})	R^2	q_e (mg·g^{-1})	K_2 (g·mg^{-1}·h^{-1})	R^2
12.02	13.10	0.373	0.994	12.90	0.0538	0.996

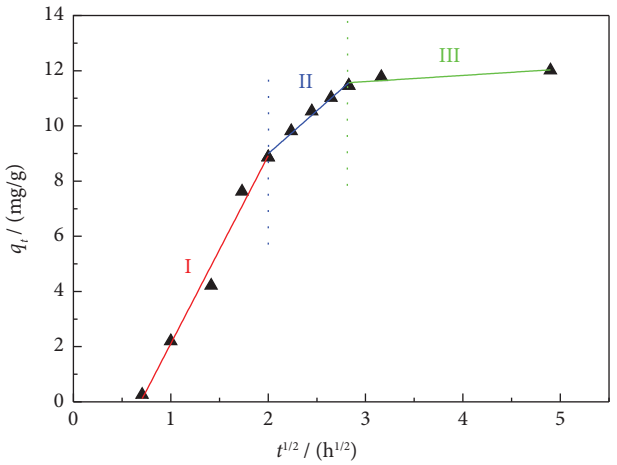

Figure 11: Linear fitting using the intraparticular diffusion model.

Table 5: Parameters of intraparticular diffusion model.

K_{dif1} (mg/g·h$^{1/2}$)	r_1	K_{dif2} (mg/g·h$^{1/2}$)	r_2	K_{dif3} (mg/g·h$^{1/2}$)	r_3
4.583	0.996	2.518	0.998	1.018	0.989

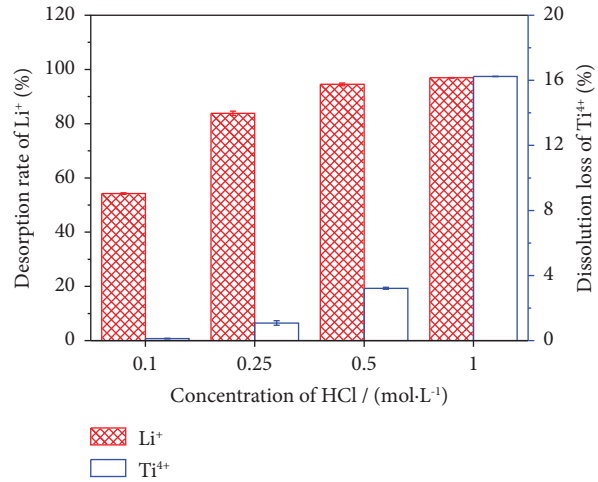

Figure 12: Effect of acidity on preparation precursor from microsphere CMC-LTO-EGDE-ME by Li^+ desorption.

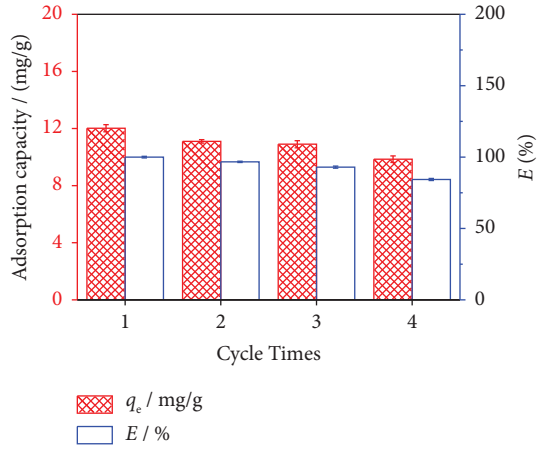

Figure 13: Regeneration performance of CMC-LTO-EGDE-ME for four-cycle times.

Table 6: Comparison of the Li^+ adsorption capacity and equilibration time at the different initial contents and water samples.

Adsorbent	Sample	Li^+ content ($mg \cdot L^{-1}$)	Adsorption capacity ($mg \cdot g^{-1}$)	Equil. time (h)	Refs.
HMO/Al_2O_3	Seawater	30	15	499	[30]
Chitosan/HMO	Seawater	30	11.4	168	[31]
$H_{1.6}Mn_{1.6}O_4$/PAN	LiCl/LiOH solution	35	10.3	24	[32]
$LiMnO_2$/PVA	LiOH solution	7	6.9	24	[33]
CTS/HMO	Geothermal water	25.78	8.98	24	[3]
HTO-400	Li^+ solution	200	34.2	24	[34]
HTO-Am	LiCl solution	300	50.03	24	[35]
$H_4Ti_5O_{12}$	Li^+ solution	500	52.97	1	[36]
CMC-HTO-EGDE	Geothermal water	25.78	12.01	8	This work

stability, and the adsorption-desorption results of five cycles are presented in Figure 13.

4. Comparison with Other Adsorption Materials

Table 6compares the materials developed in this paper with the reported adsorbents. It is worth noting that CMC-LTO-EGDE-ME can be quickly absorbed and has a high adsorption capacity for Li^+. In particular, it can be stably recycled and has an outstanding ability to recover lithium in geothermal water.

5. Conclusion

In this work, in order to improve the stability of the lithium-ion sieve, the CMC-LTO-EGDE-ME adsorption material with excellent performance was prepared by using ethylene glycol diglycidyl ether (EGDE) and melamine (ME) through the cross-linking reaction of sodium carboxymethyl

cellulose (CMC) and Li_2TiO_3 (LTO). The adsorption properties of CMC-HTO-EGDE-ME showed that the Li^+ adsorption capacity was 12.02 $mg \cdot g^{-1}$, and the equilibrium time was within 8 h. Furthermore, the adsorption kinetics can be described by the quasi-second-order model. In addition, over the pH range of 10–12, these particles have excellent Li^+ adsorption capacity. Finally, the CMC-HTO-EGDE-ME composite microspheres were applied to lithium extraction experiments in geothermal water. In the five cycles of lithium recovery experiments, the adsorption behavior and elution effect of the composite microspheres are stable, which provides a feasible technical scheme for extracting lithium from geothermal water.

Data Availability

The data used to support the findings of this study are available from the corresponding author upon request.

Conflicts of Interest

The authors declare that they have no conflicts of interest.

Acknowledgments

This study received financial support from the China National Nuclear Corporation (CNNCHN-KN-2021-0018 and BKNFY-22002060-000) and the Yangtze Scholars and Innovative Research Team in Chinese University (IRT_17R81).

References

[1] P. K. Choubey, M. S. Kim, R. R. Srivastava, J. C. Lee, and J. Y. Lee, "Advance review on the exploitation of the prominent energy-storage element: lithium. part I: from mineral and brine resources," *Minerals Engineering*, vol. 89, pp. 119–137, 2016.

[2] K. Karki, E. Epstein, J.-H. Cho et al., "Lithium-assisted electrochemical welding in silicon nanowire battery electrodes," *Nano Letters*, vol. 12, no. 3, pp. 1392–1397, 2012.

[3] L. G. Lu, X. B. Han, J. Q. Li, J. F. Hua, and M. Ouyang, "A review on the key issues for lithium-ion battery management in electric vehicles," *Journal of Power Sources*, vol. 226, pp. 272–288, 2013.

[4] H. Nie, L. Xu, D. Song et al., "$LiCoO_2$: recycling from spent batteries and regeneration with solid-state synthesis," *Green Chemistry*, vol. 17, no. 2, pp. 1276–1280, 2015.

[5] R. Chitrakar, Y. Makita, K. Ooi, and A. Sonoda, "Synthesis of iron-doped manganese oxides with an ion-sieve property: lithium adsorption from Bolivian brine," *Industrial & Engineering Chemistry Research*, vol. 53, no. 9, pp. 3682–3688, 2014.

[6] C. Grosjean, P. H. Miranda, M. Perrin, and P. Poggi, "Assessment of world lithium resources and consequences of their geographic distribution on the expected development of the electric vehicle industry," *Renewable and Sustainable Energy Reviews*, vol. 16, no. 3, pp. 1735–1744744, 2012.

[7] V. Flexer, C. F. Baspineiro, and C. I. Galli, "Lithium recovery from brines: a vital raw material for green energies with a potential environmental impact in its mining and processing," *Science of the Total Environment*, vol. 639, pp. 1188–1204, 2018.

[8] J. W. An, D. J. Kang, K. T. Tran, M. J. Kim, T. Lim, and T. Tran, "Recovery of lithium from uyuni salar brine," *Hydrometallurgy*, vol. 117-118, pp. 64–70, 2012.

[9] K. J. Kim, "Recovery of lithium hydroxide from spent lithium carbonate using crystallizations," *Separation Science and Technology*, vol. 43, no. 2, pp. 420–430, 2008.

[10] Y. J. Shih, S. K. Chien, S. R. Jhang, and Y. C. Lin, "Chemical leaching, precipitation and solvent extraction for sequential separation of valuable metals in cathode material of spent lithium-ion batteries," *Journal of the Taiwan Institute of Chemical Engineers*, vol. 100, pp. 151–159, 2019.

[11] E. G. Pinna, M. Ruiz, M. W. Ojeda, and M. H. Rodriguez, "Cathodes of spent Li-ion batteries: dissolution with phosphoric acid and recovery of lithium and cobalt from leach liquors," *Hydrometallurgy*, vol. 167, pp. 66–71, 2017.

[12] L. Sun and K. Qiu, "Organic oxalate as leachant and precipitant for the recovery of valuable metals from spent lithium-ion batteries," *Waste Management*, vol. 32, no. 8, pp. 1575–1582, 2012.

[13] M. S. a. T. D. Murodjon Samadiy and Tianlong Deng and T. L. Deng, "Lithium recovery from water resources by ion exchange and sorption method," *Journal of the Chemical Society of Pakistan*, vol. 43, no. 4, pp. 406–416, 2021.

[14] Y. L. Liu, F. Yan, H. C. Pei et al., "Preparation of PSf-g-BN15C5/NWF composite membrane with sponge-like pore structure for lithium isotopes adsorptive separation," *Journal of the Taiwan Institute of Chemical Engineers*, vol. 91, pp. 507–516, 2018.

[15] I. M. Pritula, A. V. Kosinova, O. Bezkrovnaya et al., "Linear and nonlinear optical properties of KDP crystals with incorporated Al_2O_3 nH_2O nanoparticles," *Optical Materials*, vol. 35, pp. 2429–2434, 2013.

[16] H. S. Wang, J. J. Cui, M. L. Li, Y. F. Guo, T. L. Deng, and X. P. Yu, "Selective recovery of lithium from geothermal water by EGDE cross-linked spherical CTS/LMO," *Chemical Engineering Journal*, vol. 389, Article ID 124410, 2020.

[17] X. Xu, Y. M. Chen, P. Y. Wan et al., "Extraction of lithium with functionalized lithium ion-sieves," *Progress in Materials Science*, vol. 84, pp. 276–313, 2016.

[18] K. Y. Zhao, B. J. Tong, X. P. Yu, Y. F. Guo, Y. Xie, and T. L. Deng, "Synthesis of porous fiber-supported lithium ion-sieve adsorbent for lithium recovery from geothermal water," *Chemical Engineering Journal*, vol. 430, Article ID 131423, 2022.

[19] T. F. Yi, S. Y. Yang, and Y. Xie, "Recent advances of $Li_4Ti_5O_{12}$ as a promising next generation anode material for high power lithium-ion batteries," *Journal of Materials Chemistry*, vol. 3, no. 11, pp. 5750–5777, 2015.

[20] L. A. Limjuco, G. M. Nisola, C. P. Lawagon et al., "H_2TiO_3 composite adsorbent foam for efficient and continuous recovery of Li^+ from liquid resources," *Colloids and Surfaces A: Physicochemical and Engineering Aspects*, vol. 504, pp. 267–279, 2016.

[21] L. W. Ma, B. Z. Chen, Y. Chen, and X. C. Shi, "Preparation, characterization and adsorptive properties of foam-type lithium adsorbent," *Microporous and Mesoporous Materials*, vol. 142, no. 1, pp. 147–153, 2011.

[22] G. Zhu, P. Wang, P. Qi, and C. Gao, "Adsorption and desorption properties of Li^+ on PVC-$H_{1.6}Mn_{1.6}O_4$ lithium ion-sieve membrane," *Chemical Engineering Journal*, vol. 235, pp. 340–348, 2014.

[23] R. Taurino, C. Sciancalepore, L. Collini, M. Bondi, and F. Bondioli, "Functionalization of PVC by chitosan addition:

compound stability and tensile properties," *Composites Part B: Engineering*, vol. 149, pp. 240–247, 2018.

[24] J. An, Y. Y. Ren, H. Yang et al., "Sodium carboxymethyl cellulose as an effective modifier for boosting the electrochemical performance of commercial TiO_2," *Energy Technology*, vol. 8, no. 5, Article ID 1901253, 2020.

[25] S. Barkhordari and M. Yadollahi, "Carboxymethyl cellulose capsulated layered double hydroxides/drug nanohybrids for cephalexin oral delivery," *Applied Clay Science*, vol. 121-122, pp. 77–85, 2016.

[26] D. Yuan, L. Chen, X. Xiong, L. Yuan, S. Liao, and Y. Wang, "Removal of uranium (VI) from aqueous solution by amidoxime functionalized superparamagnetic polymer microspheres prepared by a controlled radical polymerization in the presence of DPE," *Chemical Engineering Journal*, vol. 285, pp. 358–367, 2016.

[27] J. P. Simonin, "On the comparison of pseudo-first order and pseudo-second order rate laws in the modeling of adsorption kinetics," *Chemical Engineering Journal*, vol. 300, pp. 254–263, 2016.

[28] X. Yi, F. Sun, Z. Han et al., "Graphene oxide encapsulated polyvinyl alcohol/sodium alginate hydrogel microspheres for Cu(II) and U(VI) removal," *Ecotoxicology and Environmental Safety*, vol. 158, pp. 309–318, 2018.

[29] S. M. Robinson, W. D. Arnold, and C. H. Byers, "Mass-transfer mechanisms for zeolite ion exchange in wastewater treatment," *AIChE Journal*, vol. 40, no. 12, pp. 2045–2054, 1994.

[30] H. J. Hong, I. S. Park, T. Ryu, B. G. Kim, and K. S. Chung, "Macroporous hydrogen manganese oxide (HMO)/Al_2O_3 for effective lithium recovery from seawater: effects of the macroporous vs. mesopores," *Industrial & Engineering Chemistry Research*, vol. 58, no. 19, pp. 8342–8348, 2019.

[31] M. Moazeni, H. Hajipour, M. Askari, and M. Nusheh, "Hydrothermal synthesis and characterization of titanium dioxide nanotubes as novel lithium adsorbents," *Materials Research Bulletin*, vol. 61, pp. 70–75, 2015.

[32] M. J. Park, G. M. Nisola, A. B. Beltran et al., "Recyclable composite nanofiber adsorbent for Li^+ recovery from seawater desalination retentate," *Chemical Engineering Journal*, vol. 254, pp. 73–81, 2014.

[33] G. M. Nisola, L. A. Limjuco, E. L. Vivas et al., "Macroporous flexible polyvinyl alcohol lithium adsorbent foam composite prepared via surfactant blending and cryo-desiccation," *Chemical Engineering Journal*, vol. 280, pp. 536–548, 2015.

[34] X. W. Li, Y. H. Chao, L. L. Chen et al., "Taming wettability of lithium ion sieve via different TiO_2 precursors for effective Li recovery from aqueous lithium resources," *Chemical Engineering Journal*, vol. 392, Article ID 123731, 2020.

[35] X. W. Li, L. L. Chen, Y. H. Chao et al., "Amorphous TiO_2-drived large capacity lithium ion sieve for lithium recovery," *Chemical Engineering & Technology*, vol. 43, no. 9, pp. 1784–1791, 2020.

[36] X. W. Li, L. L. Chen, Y. H. Chao et al., "Highly selective separation of lithium with hierarchical porous lithium-ion sieve microsphere derived from MXene," *Desalination*, vol. 537, Article ID 115847, 2022.